Toxicon 250 (2024) 108115

Contents lists available at ScienceDirect

Toxicon

journal homepage: www.elsevier.com/locate/toxicon

An impedimetric determination of zearalenone on MIP-modified carboceramic electrode

Dilruba Küçük [a], Gülcan Üner [a], Semih Latif İpek [a,b,**], Mustafa Oguzhan Caglayan [c], Zafer Üstündağ [a,*]

[a] Kutahya Dumlupınar University, Chemistry Department, Kütahya, Turkey
[b] Adana Alparslan Türkeş Science and Technology University, Department of Food Eng., Adana, Turkey
[c] Bilecik Şeyh Edebali University, Bioengineering Department, Bilecik, Turkey

ARTICLE INFO

Handling editor: Denise Tambourgi

Keywords:
Zearalenone
Mycotoxin
Electrochemical impedance spectroscopy
Molecularly imprinted polymer

ABSTRACT

Zearalenone (ZEN) is a mycotoxin that poses significant risks to human and animal health due to its mutagenic, immunosuppressive, and carcinogenic properties. This study presents a novel analytical method for detecting ZEN using electrochemical impedance spectroscopy (EIS) combined with a molecularly imprinted polymer (MIP). ZEN, used as the template molecule, was incorporated into polypyrrole on screen-printed electrodes (SPE), and a ZEN-sensitive MIP sensor was created through template removal. The modified sensor surfaces were characterized by EIS and scanning electron microscopy (SEM). An impedimetric MIP sensor for ZEN was developed, offering a detection range from 1 pM to 500 pM. The method's limit of detection (LOD) was established at 1 pM (0.3 pg/mL) with a signal-to-noise ratio of 3 (S/N = 3). The method demonstrated high precision and accuracy, with a maximum relative standard deviation (RSD) of less than 4.4% at a 95% confidence level, and relative error (RE) values ranging from −0.8% to −2.7%. The selectivity of the developed MIP sensor was evaluated using ochratoxin A, ochratoxin B, and aflatoxin B1, with no significant interference observed. ZEN recovery from spiked samples was between 95% and 105%, indicating that the method was successfully applied to grain samples, including corn, rice, and wheat.

1. Introduction

Mycotoxins are secondary metabolites produced by fungi, known for their various toxic effects on humans, animals, and plants. Zearalenone (ZEN), a mycotoxin, is a secondary metabolite synthesized by fungi of the *Fusarium* genus, including species such as *Fusarium graminearum*, *Fusarium culmorum*, *Fusarium cerealis*, *Fusarium equiseti*, *Fusarium crookwellense*, and *Fusarium semitectum* (Gadzała-Kopciuch et al., 2011). *Fusarium* fungi infect and proliferate on crops both in the field and during storage, resulting in varying levels of contamination by the ZEN mycotoxin produced by these fungi. ZEN is a common contaminants in cattle feed and food stocks, frequently contaminating crops like corn, wheat, and barley (Zhang et al., 2023). Since ZEN cannot be eliminated during production, the entire food chain is directly or indirectly affected by ZEN contamination. Consequently, ZEN negatively impacts crop production globally, causing significant economic losses (Ji et al., 2023). In North and Central America alone, over 10 million tons of corn, wheat, and other crop flours are contaminated with ZEN each year (De Rycke et al., 2021; Ji et al., 2023). Humans are exposed to the ZEN toxin through the consumption of products such as grains, meat, milk, dried fruits and vegetables, beer, and wine (Bauer et al., 2016; Carballo et al., 2019; Döll and Dänicke, 2011; Kowalska et al., 2016).

Due to its structure resembling natural estrogen hormones, ZEN has been proven through numerous animal experiments to disrupt endocrine hormone balance in humans and is therefore known as an endocrine-disrupting chemical (De Rycke et al., 2021; Kowalska et al., 2016). According to European Food and Safety Authority (EFSA), ZEN is classified as mutagenic, carcinogenic, teratogenic, estrogenic and genotoxic, hepatotoxic, hematotoxic, immunotoxic, nephrotoxic, dermatotoxic, and neurotoxic (Garcia et al., 2023; Han et al., 2022). Moreover, while classified by IARC in Group 3 as non-carcinogenic, two rodent carcinogenicity bioassays have observed significant increases in pituitary and hepatic adenomas following exposure to ZEN (Chain, 2011; Garcia et al., 2023). In response to the risks posed by ZEN, the EFSA's Scientific Panel

* Corresponding author.
** Corresponding author. Kutahya Dumlupınar University, Chemistry Department, Kütahya, Turkey.
E-mail addresses: slipek@atu.edu.tr (S.L. İpek), zustundag@gmail.com (Z. Üstündağ).

https://doi.org/10.1016/j.toxicon.2024.108115
Received 18 August 2024; Received in revised form 18 September 2024; Accepted 1 October 2024
Available online 3 October 2024

on Contaminants in the Food Chain has set a tolerable daily intake (TDI) value of 0.250 ng/mL body weight/day for humans (EFSA Panel on Contaminants in the Food Chain, 2011). Maximum residue limits for ZEN in cereal products and corn can be found in Table 1 (Kowalska et al., 2016; Kyprianou, 2007).

Standard analysis method for ZEN contamination relies on chromatographic techniques (Radi et al., 2020; Xu et al., 2020). However, since these techniques can be costly and time consuming, developed ZEN detection methods has expanded in recent years to include electrochemical, optical, and spectroscopic methods (Caglayan et al., 2022). Various methods for ZEN detection are given in Table S1. Spectroscopic methods (Li et al., 2018; Zhang et al., 2015, 2018, 2020), imaging surface plasmon resonance (iSPR) (Dorokhin et al., 2011; Hossain and Maragos, 2018; Joshi et al., 2016), and ellipsometry (Abid-Essefi et al., 2004; Nabok et al., 2011) have been studied for ZEN analysis in the literature. Moreover, electrochemical methods have been extensively researched for the detection of ZEN. Amperometric assays utilizing antibodies have been developed and applied to various samples (Feng et al., 2013; Hervás et al., 2009; Panini et al., 2010, 2011; Xu et al., 2017). Another method involves direct amperometric detection of ZEN using a carbon paste electrode modified with carbon nanotubes (Afzali et al., 2015). Additionally, aptamer-based amperometric techniques have been employed for ZEN detection (Ji et al., 2019). Impedance methods for ZEN analysis have been developed using antibodies or molecularly imprinted polymers (Gu et al., 2015; Hervás et al., 2010). Voltammetric techniques have also been explored for ZEN determination, including direct (Nasir and Pumera, 2014), antibody-based (Liu et al., 2014), and aptamer-based approaches (Azri et al., 2020; He and Yan, 2019; Ma et al., 2019). Specifically, electrochemical impedance spectroscopy (EIS) has emerged as a highly sensitive technique for ZEN analysis, leveraging antibodies, aptamers, or molecular imprinting for enhanced detection (Caglayan and Üstündağ, 2020). Carbon-ceramic (carboceramic, CC) material refers to a composite formed by blending a carbon-based material with a substance that transforms into ceramic when subjected to high temperatures under an inert atmosphere. In this study, coal tar pitch (CTP) and a flux material (F-102, from Çinikop Co., Turkey) were utilized as carbon sources and ceramic precursors. The commercial dust F-102 comprises oxides of Na and Al, as well as Zn, Pb, Zr, Si, and Bi. An affordable, conductive, and original CC material was developed and applied to modify the surface of screen-printed electrodes. In this study, a molecularly imprinted polymer (MIP) surface was also used as a diagnostic element. Polypyrrole (pPy) was selected for this purpose due to its biocompatibility, electrical conductivity, and stability (Kong et al., 2010). The MIP layer was created by electropolymerizing pyrrole with the template molecule ZEN, and for the first time, ZEN detection was performed on the resulting modified electrodes using electrochemical impedance spectroscopy (EIS).

Table 1
Maximum residue limit for ZEN (Kowalska et al., 2016; Kyprianou, 2007).

Source	Maximum level (ng/mL)
Unprocessed grains other than corn	100
Unprocessed corn	350
Cereals intended for direct human consumption, flour, bran intended for direct human consumption, and seeds	75
Refined corn oil	400
Bread (including small bakery products), pastries, biscuits, cereal snacks, and breakfast cereals (excluding corn snacks and corn-based breakfast cereals)	50
Corn intended for direct human consumption, corn-based snacks, and corn-based breakfast cereals	100
Processed corn and grain-based foods for babies, children, and adolescents	20

2. Experimental

2.1. Chemicals and materials

The chemical reagents used in this study were obtained from Sigma-Aldrich and Merck and purchased from their local distributors. Ultrapure water (UPW) with a resistivity of 18.2 MΩ cm was utilized for all aqueous solutions and washing steps. Zearalenone (ZEN, 6-[10-hydroxy-6-oxo-trans-1-undecenyl]-β-resorcyclic acid lactone), flux (F-102), CTP (CSense, Turkey), and other chemicals were used without further purification unless stated otherwise.

All electrochemical experiments were conducted at 23 ± 3 °C using screen-printed electrodes (SPEs) (CSense, Turkey, C 200, graphite working electrode diameter is 4 mm) with a Gamry Reference 300 (USA) electrochemical analyzer. Prior to use, the SPEs underwent pretreatment to remove impurities from the working electrode surface and to achieve reproducible results using linear sweep voltammetry (LSV) (scanning rate of 20 mV/s between 0 and -2 V). EIS measurements were carried out between 0.1 Hz and 300 kHz with a 5 mV amplitude and a DC potential of 0.055 V. CV measurements were performed at a scan rate of 200 mV/s with a step potential of 2 mV (Erkal-Aytemur et al., 2019; Erkal et al., 2016).

2.2. Preparation and characterization of electrodes

A homogeneous mixture of 5 g of raw coal tar pitch (r-CTP) and 5 g of F-102, with a minimal amount of acetone, was prepared and pyrolyzed in a tube furnace (Protherm, USA) at 1000 °C under a nitrogen atmosphere, using a heating rate of 10 °C/min for 1 h, following the method described elsewhere (Erkal et al., 2016). The carbonized material was ground using a ball mill with alumina balls (Retsch, PM200, Germany) at 500 rpm for 1 h to reduce particle size. One gram of the ground CC was mixed with 25 mL of acetone to create a conductive ink. This ink (20 μL) was applied to the electrode surface and dried under an IR lamp (75 W) for 5 min, producing the electrode referred to as SPE-CC.

The SPE-CC electrode was then exposed to a positive scan in a solution containing 1.0 μM ZEN (dissolved in minimal ethanol) and 50 mM Py in 0.1 M KCl. During this process, the template molecule, ZEN, entrapped in polymerized Py (Işık et al., 2021). The resulting SPE-CC-ZEN electrode was immersed in a 0.5 M HCl solution for 10 min and then sonicated for 1 min to remove ZEN molecules from the electrode surface (Işık et al., 2021). The electrode surface obtained after removing the ZEN molecules was designated SPE-CC-ZEN*. For comparison, an electrode was prepared by polymerizing pyrrole on the SPE-CC surface alone, referred to as SPE-CC-pPy.

All prepared electrode surfaces were characterized by electrochemical impedance spectroscopy (EIS) in a solution of 1 mM $K_4Fe(CN)_6/K_3Fe(CN)_6$ redox probe pair in 0.1 M KCl.

The surface morphologies of the SPE-CC-pPy, SPE-CC-ZEN, and SPE-CC-ZEN* electrodes were examined using scanning electron microscopy and energy dispersive X-ray spectroscopy (SEM and EDX, Nova, NanoSEM-650, Belgium). Additionally, the XRD patterns of the CTP and the CC materials were obtained using an X-ray diffractometer (Rigaku, Miniflex, Japan) for further characterization.

2.3. Development of an electroanalytical method for ZEN detection

Standard ZEN solutions were prepared at concentrations of 1, 2, 5, 12, 30, 75, 200, and 500 pM in 0.1 M PBS (phosphate buffer solution) with a pH of 7. These solutions were then applied to the SPE-CC-ZEN* electrode. After a 30-min incubation, the electrodes were washed with pure water, followed by the addition of a redox probe couple solution for EIS measurements. Impedimetric analyses were conducted using a 1 mM $K_3Fe(CN)_6/K_4Fe(CN)_6$ redox probe couple.

A calibration curve was constructed based on the Rct values obtained from the Nyquist plots of the electrodes treated with ZEN solutions.

Calibration studies were performed five times, with standard deviation error bars included. The limit of detection (LOD) was calculated using the maximum σ value at a 95% confidence level (3σ = 0.017).

2.4. Electrode stability

The stability of the SPE-CC-ZEN* electrode was evaluated by repeatedly measuring 10 pM ZEN. After each measurement, ZEN was removed using 0.5 M HCl and reloaded onto the electrode. This process was repeated for at least ten consecutive measurements to assess sensor stability.

To further assess sensor stability, recovery % values were calculated from the Nyquist plots obtained from measurements conducted on the same day and over five consecutive days (N = 5), after treating the SPE-CC-ZEN* surface with 10 pM ZEN.

Additionally, the developed analytical method was validated by performing sensitivity and accuracy tests using a 10 pM ZEN concentration. The results were analyzed using intraday and interday experiments over five days.

2.5. Interference studies

Interference studies were performed to assess the impact of potential interfering agents, including ochratoxin A (OTA), ochratoxin B (OTB), and aflatoxin B1 (AFB1), on the sensor's response to 10 pM ZEN. The Rct % values were determined based on the sensor's response to these agents. The experiments involved adding 200 pM of the potential interfering agents to the ZEN analyte samples.

2.6. Real sample tests

To evaluate the performance of the developed detection method on real samples, corn, wheat, and rice samples were used. Five grams of each ground grain sample was sonicated at room temperature for 30 min in a mixture of 20 mL methanol (80:20). The resulting supernatant was centrifuged, and the clear solution obtained was adjusted to pH 7 using PBS (Liu et al., 2024). Measurements were taken by spiking the real sample solutions with 10, 50, and 200 pM ZEN, and recovery values were obtained (N = 5).

3. Results and discussion

3.1. Preparation and characterization of SPE-CC-ZEN imprinted polymer electrodes

Fig. 1 presents the cyclic voltammogram (CV) of 50 mM pyrrole in 0.1 M KCl, scanned at a rate of 200 mV/s over 5 cycles. In the first scan, an oxidation peak was observed at approximately 0.65 V. In the second cycle, a significant decrease in the peak current was noted, and by the fifth cycle, the current had stabilized. The decrease in peak current after the first scan is believed to be due to the continuous accumulation of pPy films on the electrode surface, which likely restricts the access of the monomer to the surface (Işık et al., 2021; Uygun and Dilgin, 2013).

During the formation of the electrode referred to as SPE-CC-ZEN*, the removal of ZEN molecules from the pPy film was achieved by immersing the SPE-CC-ZEN electrode in a 0.5 M HCl solution for 10 min, followed by sonication for 1 min (Işık et al., 2021).

Additionally, to confirm the non-specific binding of ZEN molecules to the polymer matrix, an electrode with a pPy surface (SPE-CC-pPy) was developed using the same electropolymerization conditions without ZEN molecules.

The surface morphologies of the SPE-CC-pPy, SPE-CC-ZEN, and SPE-CC-ZEN* electrodes is shown in Fig. 2. As can be seen from the SEM images, the material is sub-micron in size (micro- and nanomaterial). Fig. S1 presents the EDX spectrum and elemental composition distribution of the CC. The spectrum shows the elemental content of the CC,

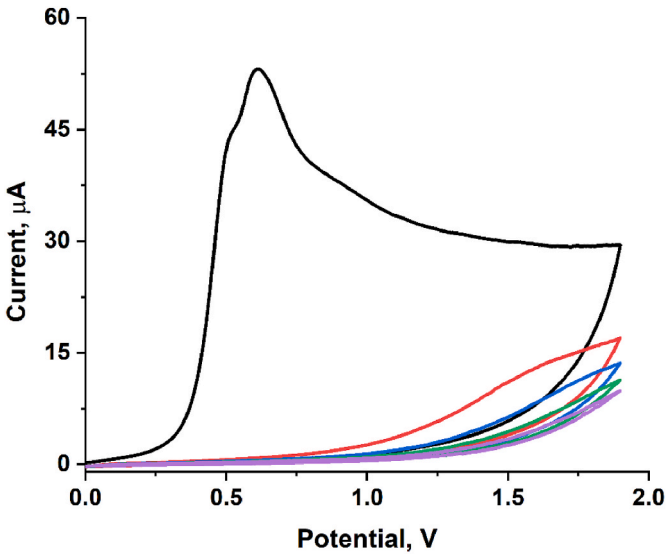

Fig. 1. Cyclic voltammogram of 50 mM pyrrole (in 0.1 M KCl) at a scan rate of 200 mV/s.

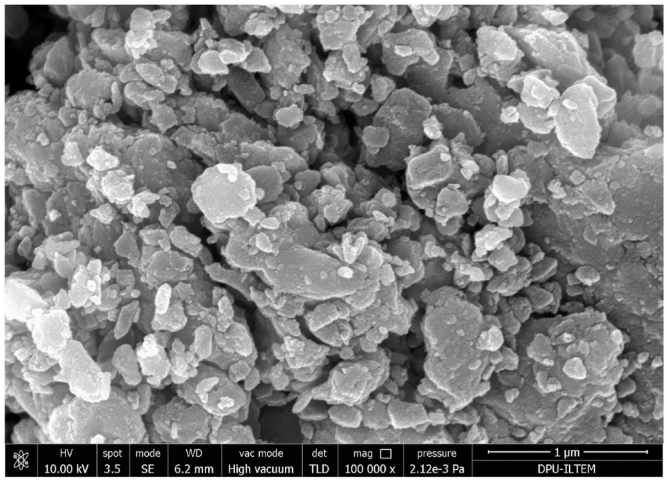

Fig. 2. SEM image of the CC material obtained by pyrolyzing the coal tar-flux.

including 10.95% B, 7.87% Zn, 11.53% Si, 6.99% Pb, and 9.05% Bi, by weight. This elemental composition originates from the F102 component of the CC.

XRD patterns of CTP and CC materials are shown in Figures S2 and Figure S3. The pattern in Fig. S2 matches the literature data for pyrolyzed carbon materials (Khalil et al., 2013), showing a typical carbon main peak at approximately 2Θ = 25°. Fig. S3 displays the crystal structure of the CC material, and indicates that the CC composite has a polycrystalline structure.

In Fig. S4 the SEM image of the SPE-CC-pPy electrode obtained by pyrrole modification on the SPE-CC electrode surface is shown. Compared to SEM image of CC (Fig. 2), a rougher surface structure has formed, with these grains being at the nanoscale and arranged in a repetitive pattern.

Fig. S5, shows the SEM image of the SPE-CC-ZEN surface obtained by modifying the SPE-CC electrode with 1 µM ZEN and 50 mM pyrrole. The SEM image of the SPE-CC-ZEN surface is very similar to that of the SPE-CC-pPy surface shown in Fig. S4. Fig. S6 displays the SEM image of the SPE-CC-ZEN* electrode, which was obtained by removing ZEN molecules from the ZEN-imprinted SPE-CC-ZEN electrode. No significant difference is observed between these SEM images; however, a

comparison of the MIP and non-imprinted polymer structures using an impedimetric method has also been conducted.

EIS characterizations of all modified SPE surfaces were conducted using a 1 mM $K_4Fe(CN)_6/K_3Fe(CN)_6$ redox probe pair in 0.1 M KCl. The impedance measurements were performed over a frequency range of 0.2 Hz–300 kHz at a DC potential of 0.05 V. Fig. 3 shows the Nyquist plots for the redox couple on the surfaces of SPE, SPE-CC, SPE-CC-ZEN (1 μM), SPE-CC-ZEN*, and the SPE-CC-ZEN* electrode treated with 1 pM ZEN (SPE-CC-ZEN (1 pM)) for calibration. All Nyquist plots were fitted to a Warburg impedance model (Zw) combined with a constant phase element (CPE) circuit to account for diffusion effects in all electrodes (Aşık et al., 2022; Erkal et al., 2014; Saygılı-Canlıdinç et al., 2023). The Nyquist plot of the redox couple obtained from the CTP-CC electrode surface, along with the electrical equivalent circuit model and the fitted curve, is presented in Fig. S7. Fig. S8 shows a comparison of the electron transfer resistances (Rct) for the redox probe pair, as determined from the fitted Nyquist plots (Üstündağ and Erkal, 2017). The data reveal that the SPE-CC electrode surface exhibits the lowest electron transfer resistance for the redox couple. In contrast, the redox couple's charge transfer resistance is highest on the ZEN-imprinted electrode, which is consistent with expectations (Işık et al., 2021).

3.2. Electroanalytical performance of the developed MIP sensor

SPE-CC-ZEN* electrodes were prepared with optimized parameters to establish the sensor's calibration curve and analytical performance metrics. The detection range was evaluated from 1 pM to 500 pM. Impedimetric analyses were performed after a 30-min incubation in a 1 mM $K_3Fe(CN)_6/K_4Fe(CN)_6$ redox probe at pH 7. Nyquist plots for electrodes treated with ZEN solutions at various concentrations are shown in Fig. 4, while the semi-logarithmic calibration curve is presented in Fig. 5.

Based on the calibration curve data, the equation for the developed method is Rct (kΩ) = 1.5993 + 2.6793log[ZEN, pM], with a limit of detection (LOD) of 1 pM. The analytical data obtained from regression analysis are presented in Table 2.

3.3. Electrode stability

The stability of the SPE-CC-ZEN* electrode was evaluated by treating it with 10 pM ZEN, then removing and reloading ZEN with 0.5 M HCl. The electrode demonstrated stable performance across at least ten consecutive measurements. Nyquist plots shown in Fig. S9 reveal that

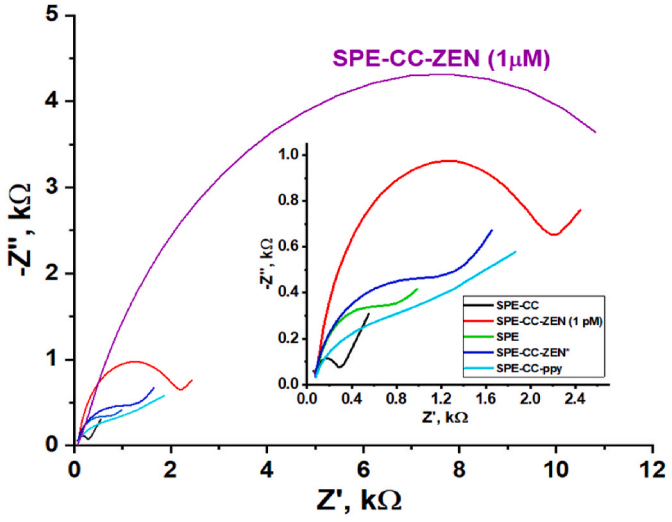

Fig. 3. Nyquist plots of 1 mM $K_4Fe(CN)_6/K_3Fe(CN)_6$ (in 0.1 M KCl) on the prepared electrodes.

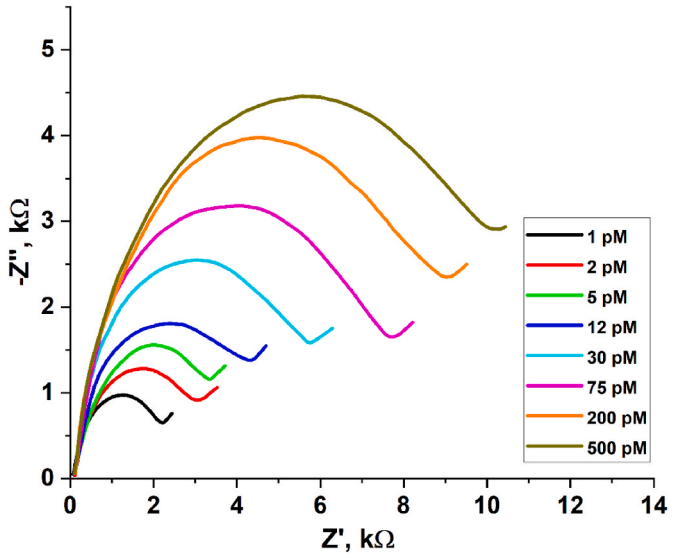

Fig. 4. Nyquist plots obtained from the SPE-CC-ZEN* surface after treatment with various concentrations of ZEN in 1 mM $K_4Fe(CN)_6/K_3Fe(CN)_6$ (in 0.1 M KCl).

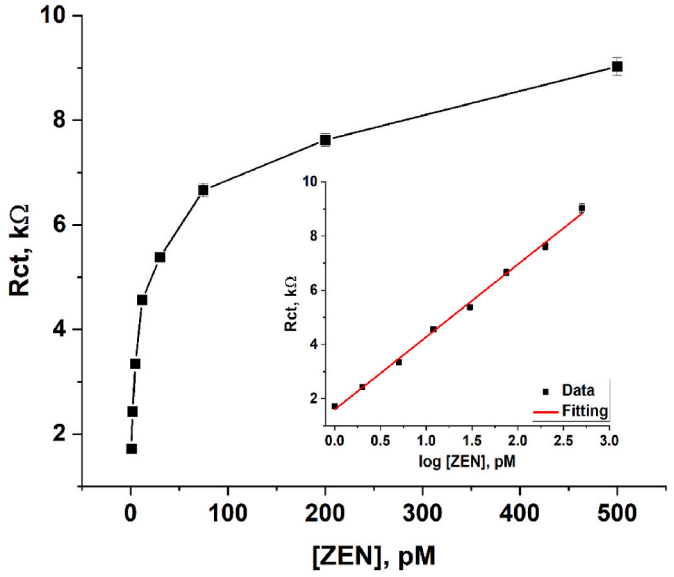

Fig. 5. Calibration curve and semi-logarithmic linear plot.

Table 2
Analytical parameters of the developed method (N = 5).

Analytic parameter	Value
Equation (kΩ, pM)	Rct = 1.5993 + 2.6793log[ZEN]
Standard error of slope, kΩ/pM	0.0581
Standard error of intercept, kΩ	0.0919
R^2	0.9972
Range, pM	1–500
Range, pg/mL	0.3–160
3xSD, kΩ	0.051
Detection limit, LOD, pM (S/N = 3)	1.0
Detection limit, LOD, pg/mL	0.3

the initial measurement with a 10 pM standard sample yielded a resistance of 4.2718 kΩ. The calculated concentration values and recovery percentages are provided in Table 3. The results indicate that the sensor, after sequentially removing and reloading 10 pM ZEN, maintained a

Table 3
Intraday and interday stability measurements of the sensor for 10 pM ZEN standard. Results for five consecutive uses within a day and for five consecutive days (N = 5).

Parameter	Result for	Measured Rct, kΩ	Calculated, pM	Recovery %
Interday	1st use	4.272 ± 0.091	9.82	98.24
	5th use	4.281 ± 0.151	10.02	100.02
Intraday	1st day	4.273 ± 0.073	9.95	99.54
	5th day	4.254 ± 0.093	9.79	97.93

recovery percentage of 95% within acceptable limits for intraday measurements over five consecutive uses. Interday stability tests were conducted over five successive days.

3.4. Precision and accuracy studies

To evaluate the precision, accuracy, and selectivity of the developed sensor, intraday and interday precision and accuracy measurements were conducted using 10 pM ZEN on five independent samples. Additionally, interday precision was assessed over five consecutive days. Table 4 presents the relative error percentages (RE%) as measures of both intraday and interday precision and accuracy. The maximum RSD % value of 4.37 (<5%, for a 95% confidence level) indicates that the method is highly precise and accurate. The RE% values ranging from −0.79 to −2.74 demonstrate that the method has a high level of accuracy.

3.5. Selectivity and real sample application

Interference experiments were conducted using 200 pM OTA, OTB, and AFB1 to assess potential interference with 10 pM ZEN. The sensor signal changes were found to be less than 4.5%. The Rct% change graph derived from the sensor response is shown in Fig. S10.

The sensor performance on real samples was evaluated using 10, 50, and 200 pM ZEN spiked into grain samples. Recovery values for ZEN spiked into the real sample solutions were found to be reasonably high, ranging from 95% to 105% (N = 5). Since the RSD% values for the spiked samples were also below 5%, it was concluded that the measurements for real sample analysis have high precision (Table 5). Additionally, these results showed good correlation with the accuracy and precision obtained from ZEN in the buffer solution.

4. Conclusion

In this study, we demonstrated for the first time the use of a CC material, produced using flux and coal tar, for electrode modification. We also applied a method using EIS to achieve a detection limit for ZEN at low concentrations. This is the first development of an MIP-CC electrode, establishing its applicability for ZEN detection. The impedimetric method and MIP-based sensing element we developed allow for the detection of ZEN within a concentration range of 1–500 pM, with a LOD of 1 pM. The sensor demonstrated precision and accuracy that meet analytical performance criteria. Furthermore, the sensor's selectivity was evaluated against potential toxins, such as OTA, OTB, and AFB1, showing high selectivity towards ZEN with signal variations remaining within ±5%. To assess the sensor's performance with real samples, a standard addition method was used. The sensor's analytical performance was minimally affected by the real sample matrix, with recovery values ranging from 95% to 105%. Thus, the sensor's effectiveness for the electrochemical detection of ZEN was confirmed.

CRediT authorship contribution statement

Dilruba Küçük: Resources, Methodology, Investigation, Formal analysis. **Gülcan Üner:** Writing – original draft, Validation, Investigation, Formal analysis. **Semih Latif İpek:** Writing – original draft, Supervision, Resources, Methodology, Conceptualization. **Mustafa Oguzhan Caglayan:** Writing – review & editing, Writing – original draft, Validation, Resources, Methodology, Data curation, Conceptualization. **Zafer Üstündağ:** Writing – original draft, Validation, Supervision, Project administration, Funding acquisition, Data curation, Conceptualization.

Table 4
Intraday and interday precision and accuracy values obtained for 10 pM ZEN over five consecutive days (N = 5).

	Analytical parameter	Values
Intraday	found, pM	9.92 ± 0.12
	RSD %	1.18
	RE %	−0.79
Interday	found, pM	9.73 ± 0.43
	RSD %	4.37
	RE %	−2.74

*RE: relative error, RSD: relative standard deviation.

Table 5
Analytical evaluation of the real sample application of the developed method (N = 5).

Sample	Spiked, pM	Found, pM	RSD %	Recovery %
Corn	10	9.8 ± 0.2	2.0	98.0
	50	47.8 ± 1.4	2.9	95.6
	200	195.2 ± 4.3	2.2	97.6
Rice	10	10.3 ± 0.3	2.9	103.0
	50	52.4 ± 2.3	4.4	104.8
	200	196.8 ± 5.8	2.9	98.4
Wheat	10	9.7 ± 0.3	3.1	97.0
	50	49.5 ± 1.68	3.4	99.0
	200	192.3 ± 8.6	4.5	96.2

Declaration of competing interest

The authors declare that they have no known competing financial interests or personal relationships that could have appeared to influence the work reported in this paper.

Data availability

Data will be made available on request.

Acknowledgment

This study was supported by the TUBITAK 2209-A - Research Project Support Program, under project number 1919B012108952. Additionally, the authors would like to thank Kütahya Dumlupınar University for the financial contribution to this study through the BAP project numbered 2022–60.

Appendix A. Supplementary data

Supplementary data to this article can be found online at https://doi.org/10.1016/j.toxicon.2024.108115.

References

Abid-Essefi, S., Ouanes, Z., Hassen, W., Baudrimont, I., Creppy, E., Bacha, H., 2004. Cytotoxicity, inhibition of DNA and protein syntheses and oxidative damage in cultured cells exposed to zearalenone. Toxicol. Vitro 18, 467–474.
Afzali, D., Padash, M., Mostafavi, A., 2015. Determination of trace amounts of zearalenone in beverage samples with an electrochemical sensor. Mycotoxin Res. 31, 203–208.
Aşık, İ., Üstündağ, Z., Kariper, İ.A., 2022. Electroanalytical determination of Sudan I using gold nanoparticle/graphene nanoribbons-modified glassy carbon electrode. Electrocatalysis 13, 338–347.

Azri, F.A., Eissa, S., Zourob, M., Chinnappan, R., Sukor, R., Yusof, N.A., Raston, N.H.A., Alhoshani, A., Jinap, S., 2020. Electrochemical determination of zearalenone using a label-free competitive aptasensor. Microchim. Acta 187, 266.
Bauer, J.I., Gross, M., Gottschalk, C., Usleber, E., 2016. Investigations on the occurrence of mycotoxins in beer. Food Control 63, 135–139.
Caglayan, M.O., Şahin, S., Üstündağ, Z., 2022. Detection strategies of zearalenone for food safety: a review. Crit. Rev. Anal. Chem. 52, 294–313.
Caglayan, M.O., Üstündağ, Z., 2020. Detection of zearalenone in an aptamer assay using attenuated internal reflection ellipsometry and it's cereal sample applications. Food Chem. Toxicol. 136, 111081.
Carballo, D., Tolosa, J., Ferrer, E., Berrada, H., 2019. Dietary exposure assessment to mycotoxins through total diet studies. A review. Food Chem. Toxicol. 128, 8–20.
Chain, E., 2011. Scientific Opinion on the risks for public health related to the presence of zearalenone in food. EFSA J. 9, 2197.
De Rycke, E., Foubert, A., Dubruel, P., Bol'hakov, O.I., De Saeger, S., Beloglazova, N., 2021. Recent advances in electrochemical monitoring of zearalenone in diverse matrices. Food Chem. 353, 129342.
Dorokhin, D., Haasnoot, W., Franssen, M.C., Zuilhof, H., Nielen, M.W., 2011. Imaging surface plasmon resonance for multiplex microassay sensing of mycotoxins. Anal. Bioanal. Chem. 400, 3005–3011.
Döll, S., Dänicke, S., 2011. The Fusarium toxins deoxynivalenol (DON) and zearalenone (ZON) in animal feeding. Prev. Vet. Med. 102, 132–145.
EFSA Panel on Contaminants in the Food Chain, 2011. Scientific Opinion on the risks for public health related to the presence of zearalenone in food. EFSA J. 9 (6), 2197.
Erkal-Aytemur, A., Üstündağ, İ., Kariper, İ.A., Çağlayan, M.O., Üstündağ, Z., 2019. Electrocatalytic effect of nano-wrinkled layer carbonaceous electrode: determination of folic acid by differential pulse voltammetry. Chem. Pap. 73, 1369–1376.
Erkal, A., Aşık, İ., Yavuz, S., Kariper, A., Üstündağ, Z., 2016. Biosensor application of carbonaceous nanocoil material: preparation, characterization, and determination of dopamine and uric acid in the presence of ascorbic acid. J. Electrochem. Soc. 163, H269.
Erkal, A., Erdoğan, M.S., Aşık, İ., Ekşi, H., Jeon, S., Solak, A.O., Üstündağ, Z., 2014. Electrografting and surface properties of some substituted nitrophenols on glassy carbon electrode and simultaneous Pb2+-Cd2+ analysis via assist of graphene oxide terminated surface. J. Electrochem. Soc. 161, H696.
Feng, R., Zhang, Y., Ma, H., Wu, D., Fan, H., Wang, H., Li, H., Du, B., Wei, Q., 2013. Ultrasensitive non-enzymatic and non-mediator electrochemical biosensor using nitrogen-doped graphene sheets for signal amplification and nanoporous alloy as carrier. Electrochim. Acta 97, 105–111.
Gadzała-Kopciuch, R., Cendrowski, K., Cesarz, A., Kiełbasa, P., Buszewski, B., 2011. Determination of zearalenone and its metabolites in endometrial cancer by coupled separation techniques. Anal. Bioanal. Chem. 401, 2069–2078.
Garcia, I., Valente, D., Carolino, N., Dinis, H., Sousa, R., Duarte, S.C., Silva, L.J., Pereira, A.M., Pena, A., 2023. Occurrence of zearalenone in dairy farms–A study on the determinants of exposure and risk assessment. Toxicon 225, 107051.
Gu, W., Zhu, P., Jiang, D., He, X., Li, Y., Ji, J., Zhang, L., Sun, Y., Sun, X., 2015. A novel and simple cell-based electrochemical impedance biosensor for evaluating the combined toxicity of DON and ZEN. Biosens. Bioelectron. 70, 447–454.
Han, X., Huangfu, B., Xu, T., Xu, W., Asakiya, C., Huang, K., He, X., 2022. Research progress of safety of zearalenone: a review. Toxins 14, 386.
He, B., Yan, X., 2019. An amperometric zearalenone aptasensor based on signal amplification by using a composite prepared from porous platinum nanotubes, gold nanoparticles and thionine-labelled graphene oxide. Microchim. Acta 186, 1–10.
Hervás, M., López, M.Á., Escarpa, A., 2009. Electrochemical immunoassay using magnetic beads for the determination of zearalenone in baby food: an anticipated analytical tool for food safety. Anal. Chim. Acta 653, 167–172.
Hervás, M., López, M.Á., Escarpa, A., 2010. Simplified calibration and analysis on screen-printed disposable platforms for electrochemical magnetic bead-based inmunosensing of zearalenone in baby food samples. Biosens. Bioelectron. 25, 1755–1760.
Hossain, M.Z., Maragos, C.M., 2018. Gold nanoparticle-enhanced multiplexed imaging surface plasmon resonance (iSPR) detection of Fusarium mycotoxins in wheat. Biosens. Bioelectron. 101, 245–252.
Işık, D., Şahin, S., Caglayan, M.O., Üstündağ, Z., 2021. Electrochemical impedimetric detection of kanamycin using molecular imprinting for food safety. Microchem. J. 160, 105713.
Ji, J., Yu, J., Ye, Y., Sheng, L., Fang, J., Yang, Y., Sun, X., 2023. Biodegradation methods and product analysis of zearalenone and its future development trend: a review. Food Control 145, 109469.
Ji, X., Yu, C., Wen, Y., Chen, J., Yu, Y., Zhang, C., Gao, R., Mu, X., He, J., 2019. Fabrication of pioneering 3D sakura-shaped metal-organic coordination polymers Cu@ L-Glu phenomenal for signal amplification in highly sensitive detection of zearalenone. Biosens. Bioelectron. 129, 139–146.
Joshi, S., Segarra-Fas, A., Peters, J., Zuilhof, H., Van Beek, T.A., Nielen, M.W., 2016. Multiplex surface plasmon resonance biosensing and its transferability towards imaging nanoplasmonics for detection of mycotoxins in barley. Analyst 141, 1307–1318.
Khalil, H., Jawaid, M., Firoozian, P., Rashid, U., Islam, A., Akil, H.M., 2013. Activated carbon from various agricultural wastes by chemical activation with KOH: preparation and characterization. J. Biobased Mater. Bioenergy 7, 708–714.
Kong, Y., Zhao, W., Yao, S., Xu, J., Wang, W., Chen, Z., 2010. Molecularly imprinted polypyrrole prepared by electrodeposition for the selective recognition of tryptophan enantiomers. J. Appl. Polym. Sci. 115, 1952–1957.
Kowalska, K., Habrowska-Górczyńska, D.E., Piastowska-Ciesielska, A.W., 2016. Zearalenone as an endocrine disruptor in humans. Environ. Toxicol. Pharmacol. 48, 141–149.
Kyprianou, M., 2007. Commission Regulation (EC) No 1126/2007. of 28 September 2007. Amending regulation (EC) no 1881/2006 setting maximum levels for certain contaminants in foodstuffs as regards Fusarium toxins in maize and maize products. Off. J. Eur. Union 255, 14–17.
Li, Y., Chen, Q., Xu, X., Jin, Y., Wang, Y., Zhang, L., Yang, W., He, L., Feng, X., Chen, Y., 2018. Microarray surface enhanced Raman scattering based immunosensor for multiplexing detection of mycotoxin in foodstuff. Sensor. Actuator. B Chem. 266, 115–123.
Liu, L., Chao, Y., Cao, W., Wang, Y., Luo, C., Pang, X., Fan, D., Wei, Q., 2014. A label-free amperometric immunosensor for detection of zearalenone based on trimetallic Au-core/AgPt-shell nanorattles and mesoporous carbon. Anal. Chim. Acta 847, 29–36.
Liu, W., Luo, X., Wang, R., Li, Y., Zhang, H., Wang, T., Feng, W., 2024. Molecular imprinting of rice husk-derived mesoporous silica for purification and determination of zearalenone. Food Biosci. 59, 103929.
Ma, L., Bai, L., Zhao, M., Zhou, J., Chen, Y., Mu, Z., 2019. An electrochemical aptasensor for highly sensitive detection of zearalenone based on PEI-MoS2-MWCNTs nanocomposite for signal enhancement. Anal. Chim. Acta 1060, 71–78.
Nabok, A., Tsargorodskaya, A., Mustafa, M., Szekacs, I., Starodub, N., Szekacs, A., 2011. Detection of low molecular weight toxins using an optical phase method of ellipsometry. Sensor. Actuator. B Chem. 154, 232–237.
Nasir, M.Z.M., Pumera, M., 2014. Mycotoxins: simultaneous detection of zearalenone and citrinin by voltammetry on edge plane pyrolytic graphite electrode. Electroanalysis 26, 1901–1904.
Panini, N.V., Bertolino, F.A., Salinas, E., Messina, G.A., Raba, J., 2010. Zearalenone determination in corn silage samples using an immunosensor in a continuous-flow/stopped-flow systems. Biochem. Eng. J. 51, 7–13.
Panini, N.V., Salinas, E., Messina, G.A., Raba, J., 2011. Modified paramagnetic beads in a microfluidic system for the determination of zearalenone in feedstuffs samples. Food Chem. 125, 791–796.
Radi, A.E., Eissa, A., Wahdan, T., 2020. Molecularly imprinted impedimetric sensor for determination of mycotoxin zearalenone. Electroanalysis 32, 1788–1794.
Saygılı-Canlıdinç, R., Caglayan, M.O., Kariper, İ.A., Üstündağ, Z., Şahin, S., 2023. Aptamer-based impedimetric label-free detection of bisphenol A from water samples using a gold nanoparticle-modified electrochemical nanofilm platform. J. Appl. Electrochem. 53, 2239–2248.
Uygun, Z.O., Dilgin, Y., 2013. A novel impedimetric sensor based on molecularly imprinted polypyrrole modified pencil graphite electrode for trace level determination of chlorpyrifos. Sensor. Actuator. B Chem. 188, 78–84.
Üstündağ, İ., Erkal, A., 2017. Determination of dopamine in the presence of ascorbic acid on digitonin-doped coal tar pitch carbonaceous electrode. Sensor. Mater. 29.
Xu, J., Chi, J., Lin, C., Lin, X., Xie, Z., 2020. Towards high-efficient online specific discrimination of zearalenone by using gold nanoparticles@ aptamer-based affinity monolithic column. J. Chromatogr. A 1620, 461026.
Xu, W., Qing, Y., Chen, S., Chen, J., Qin, Z., Qiu, J., Li, C., 2017. Electrochemical indirect competitive immunoassay for ultrasensitive detection of zearalenone based on a glassy carbon electrode modified with carboxylated multi-walled carbon nanotubes and chitosan. Microchim. Acta 184, 3339–3347.
Zhang, W., Tang, S., Jin, Y., Yang, C., He, L., Wang, J., Chen, Y., 2020. Multiplex SERS-based lateral flow immunosensor for the detection of major mycotoxins in maize utilizing dual Raman labels and triple test lines. J. Hazard Mater. 393, 122348.
Zhang, X., Wang, X., Sun, M., Zhang, X., Song, H., Yan, Y., Sun, J., Li, X., Fang, W., 2015. A magnetic nanoparticle based enzyme-linked immunosorbent assay for sensitive quantification of zearalenone in cereal and feed samples. Toxins 7, 4216–4231.
Zhang, Y., Lu, T., Wang, Y., Diao, C., Zhou, Y., Zhao, L., Chen, H., 2018. Selection of a DNA aptamer against zearalenone and docking analysis for highly sensitive rapid visual detection with label-free aptasensor. J. Agric. Food Chem. 66, 12102–12110.
Zhang, Y., Ouyang, B., Zhang, W., Guang, C., Xu, W., Mu, W., 2023. An overview of chemical, physical and biological methods for zearalenone elimination: recent advances and future prospective. Food Control, 110011.